Bachelor's thesis

NTNU
Norwegian University of Science and Technology
Faculty of Natural Sciences
Department of Physics

Bjørn Norstrøm

Quantum Tunneling through Anti Reflection coated Superlattices

Bachelor's thesis in Physics
Supervisor: Jon Andreas Støvneng
April 2024

NTNU
Norwegian University of
Science and Technology

Bjørn Norstrøm

Quantum Tunneling through Anti Reflection coated Superlattices

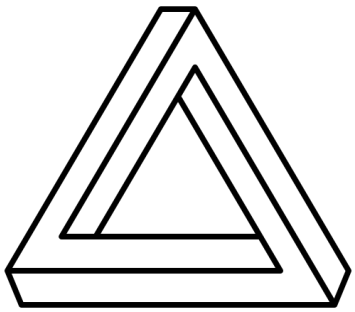

Bachelor's thesis in Physics
Supervisor: Jon Andreas Støvneng
April 2024

Norwegian University of Science and Technology
Faculty of Natural Sciences
Department of Physics

NTNU
Norwegian University of
Science and Technology

Abstract

Superlattices with the anti reflection coating used in this article, have the interesting property that they yield 100% and 0% transmission for spectra of energies. This property makes it possible to have nearly 100% of electron wave packets tunnel through, or have nearly 100% of electron wave packets reflected.Studying this, we operated within the tight binding model, running simulations and calculating transmission spectras for these anti reflection coated superlattices (ARSLs) in python. It was investigated how the transmission spectra for these ARSLs behaves with the introduction of a single potential barrier placed behind. It was concluded that the transmission spectrum follows the spectrum of the barrier in the regions the ARSL yields 100% transmission and 0% transmission in the regions the ARSL yields 0% transmission. It was studied how an ARSL affects the traveling time for electron wave packets traveling through it, to which it was concluded that the wave packets traveled faster inside the ARSL. Lastly a simulation was made where an electron was trapped between two ARSLs. The electron had more than twice the necessary energy needed to escape classically, yet was stuck bouncing back and forth between barriers with potentials less than half of the energy.

Preface

The laws of quantum mechanics permits particles, lacking the kinetic energy to exist within a region, to somehow travel through it. The region is referred to as a potential barrier and the event itself is called quantum tunneling. This yields a lot of unexpected results, like for example when you hit your hand at a desk, it may go through. A classical analogy would be a rock lacking the necessary kinetic energy to reach the top of a hill, yet somehow managing to roll over it.
This behavior seems completely nonphysical, which is why most undergraduates (myself included) have come to accept the phenomena under the understanding that this only occurs rarely, and is under no circumstance something that can be guaranteed. One can sort of come close with a double barrier. A double barrier has 100% transmission for certain energies below the potential. At first glance this may seem like quantum tunneling can be guaranteed, however due to the Heisenberg uncertainty principle, no particles realistically has a specific energy, which excludes any possibility to guarantee tunneling with a double barrier. That is why anti-reflection coated superlattice's ARSLs are interesting. They may have 100% transmission probability for entire spectra of energies lower than the potential. Additionally they have the interesting property of having 0% transmission probability for energy spectra higher than the potential. Due to these unintuitive properties, I wished to obtain a deeper insight into ARSL,s by focusing my thesis on this.

My prior knowledge of quantum tunneling consisted of an introductory course in quantum mechanics where I simulated quantum tunneling through a single potential barrier, and briefly touched the theory of resonant tunneling through double barriers. Additionally, when considering the tight time-schedule to complete the thesis in under four months, the project has been quite the challenge.

I want to express a huge thanks to Jon Andreas Støvneng for agreeing to be my advisor. With his guidance, I was able to understand the tight binding model, and the solution with retarded Green's functions. He pointed me to the literature of superlattices which eventually led to my discovery of the ARSLs discussed in this thesis. His help was also very much appreciated in locating some of the errors in my code. Lastly I want to express my thanks for the many pleasant conversations we had throughout this period.

For the following, I express my thanks to various "people" who also helped me throughout this period:
Thanks to Camille Jaunsen for convincing me that sleep is important.
Thanks to Liesbeth Campbell for borrowing me her iPad, allowing me to create figure 1.
Thanks to Ellie (J. Støvneng's dog) for her cuddliness which helped me through the mental load of this project.
Lastly a huge thanks to Sam Rouppe van der Voort and John Aslak Wee Kleven for being my two bachelorbros, sharing the experiences from our separate bachelor projects.

Table of Contents

List of Figures

List of Tables

1 Introduction

A superlattice is a system consisting of many alternating barriers and wells, where each barrier has the same thickness and height and each well has the same thickness and depth (Nakagawa et al. 1985). The anti-reflection coating used in this article is taken from (Tung and Lee 1996), which adjusts the heights and depths of barriers and wells in the superlattice to follow a Gaussian distribution peaking at the center. Since we exclusively discuss this anti reflection coating, any reference to ARSL specifically refers to this coating, unless stated otherwise. With this coating, we obtain transmission spectra mainly consisting of regions with 100% transmission and 0% transmission. We use transmission spectrum to refer to the transmission probability as a function of incoming particle energy. We study the following properties of ARSLs:

- How the transmission spectra of an ARSL is affected by the introduction of a potential barrier placed behind.
- How an ARSL affects the traveling time of electron wave-packets in the case where it allows the entire wave-packet to tunnel through.
- The possibility of trapping an electron between two ARSLs with significantly lower potential than the energy of the electron.

With Epitaxial growth technology, superlattices have been physically constructed by placing ultra thin layers of different semi-conductor films on top of each other to form a chain with this potential profile (Tung and Lee 1996). With this method, it should also be possible to produce ARSLs with the properties we want to study. This makes it natural to study the tunneling phenomena from the perspective of electrons traveling through a semi-conductor. To simulate this, we use the tight binding model. Calculations of transmission spectra and simulations were done in python.

2 Theory

2.1 Predictions

To make a prediction for how transmission spectra of ARSLs are affected by the introduction of a single potential barrier, we compare it with how the transmission spectrum of a single potential barrier is affected by the introduction of another potential barrier. This creates a double barrier, which for some energies yields a higher transmittance than each barrier does individually. This effect is highlighted if the second barrier is placed further back, as this allows for higher transmittance for even more energies. Thus we also expect a non-trivial behavior when adding a potential barrier behind an ARSL.

To make predictions for the wave packet traveling time through an ARSL, we compare the system to a double barrier. When a wave packet tunnels through a double barrier at a resonant energy, it spends some extra time between the two barriers before finally coming through. This creates a time delay in comparison to a wave packet moving in a free potential. Thus it is reasonable to expect the same time delay to occur for a tunneling electron wave packet through an ARSL. Additionally, we expect the time delay to be greater the more barriers are in an ARSL.

2.2 Constructing the Tight Binding Model

To simulate quantum tunneling in a semiconductor crystal, we wish to construct a system consisting of a barrier area surrounded by two semi-infinite lattice chains. On the two chains, the potential is constant allowing transport of a "free" electron. The following sections explains how the tight binding model can be solved with retarded Green's functions to simulate this system.

2.2.1 The tight binding approximation

We consider our system as an infinite 1-dimensional lattice with a constant lattice spacing of 5Å and with lattice points representing atoms in a semiconductor crystal. The potential for this lattice is illustrated (not approximated) with square wells, close to the atoms, separated by barriers, in figure 1. The Hamiltonian describing this system may be written as

$$H = -\frac{\hbar^2}{2m}\frac{\partial^2}{\partial x} + \sum_i V_i, \tag{1}$$

where V_i is the potential near a single atom, so that the sum describes the complete potential in figure 1.

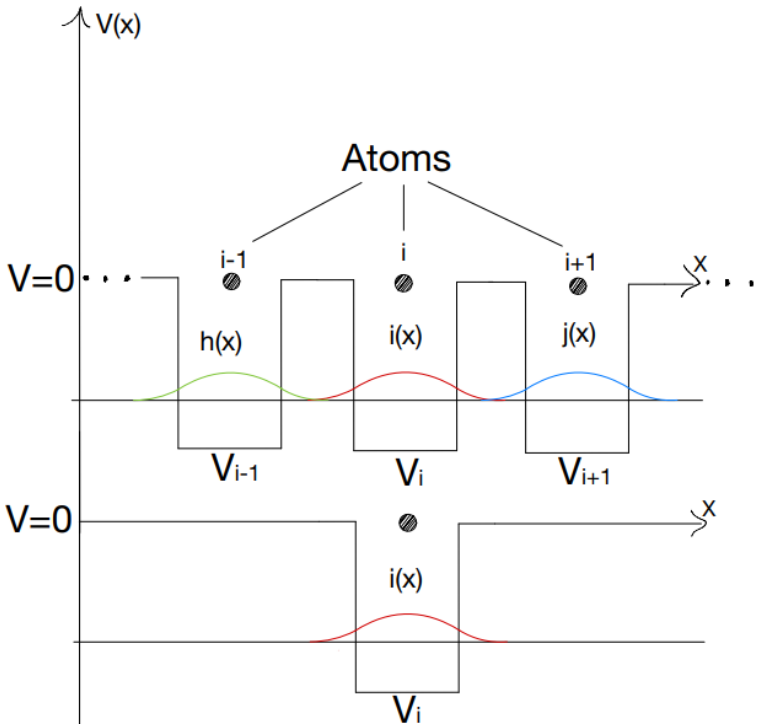

Figure 1: An illustration that shows how a wavefunction $i(x)$ for an orbital of an isolated atom can be used as a position basis for the lattice. Neighbouring wavefunctions $h(x)$ and $j(x)$ at sites $i-1$ and $i+1$ overlap with $i(x)$ inside the barriers, but (approximately) not inside the well.

We define the wavefunction $|\psi\rangle$ to describe an electron in this system. We choose a basis of wavefunctions $|i\rangle$ for $|\psi\rangle$, where $|i\rangle$ is an orbital state of an independent atom i. The time independent Schrödinger equation for this orbital state of atom i is

$$\left(-\frac{\hbar^2}{2m}\frac{\partial^2}{\partial x} + V_i(x)\right)|i\rangle = \epsilon_i|i\rangle. \tag{2}$$

Here the potential $V_i(x)$ only corresponds to a single well in figure 1 and ϵ_i is the eigenenergy of this orbital. Given that the distance between atoms is sufficiently large, we can approximate the wavefunctions $i(x)$ to be zero in neighboring wells, making this an orthogonal basis if we were to only consider the wells. This approximation is reasonable given the wavefunction in the atomic orbitals decrease exponentially with distance from the nuclei. Inside the barriers however, we do not assume the wavefunctions to vanish. This overlap is essentially what allows transport of electrons in our model (Støvneng 1991), and concludes the necessary assumptions for the Tight binding model (Kittel 2018).

2.2.2 The tight binding Hamiltonian

To find an expression for the general Hamiltonian H from eq (1), in the basis of $|i\rangle$, we apply H to $|\psi\rangle$ and obtain the following:

$$H|\psi\rangle = \left(-\frac{\hbar^2}{2m}\frac{\partial^2}{\partial x} + \sum_m V_m\right)\sum_n c_n|n\rangle. \tag{3}$$

By applying $\langle i|$ to the left we obtain the energy in well i, and get

$$\langle i|H|\Psi\rangle = \langle i|\left(-\frac{\hbar^2}{2m}\frac{\partial^2}{\partial x} + \sum_m V_m\right)\sum_n c_n|n\rangle. \tag{4}$$

In our approximation the wavefunction $i(x)$ is zero in all wells except well nr i, meaning that the only contributing potential in the Hamiltonian is V_i. Additionally the basis functions only overlap with neighboring basis functions inside the barriers, where the potential is zero. This means that the contribution from all $n \geq i+2$ and $n \leq i-2$ are zero. Eq (4) reduces to

$$\langle i|H|\psi\rangle = \langle i|\left(-\frac{\hbar^2}{2m}\frac{\partial^2}{\partial x} + V_i\right)|i\rangle + \langle i|\left(-\frac{\hbar^2}{2m}\frac{\partial^2}{\partial x}\right)|i-1\rangle + \langle i|\left(-\frac{\hbar^2}{2m}\frac{\partial^2}{\partial x}\right)|i+1\rangle. \tag{5}$$

The first term in eq (5) is ϵ_1 from eq (2). The two other terms are the energy contributions due to closeness of neighboring atomic orbitals, referred to as hopping amplitudes. We call these energy contributions $u_{i,i-1}$ and $u_{i,i+1}$ respectively, and get

$$\langle i|H|\psi\rangle = \epsilon_i + u_{i,i-1} + u_{i,i+1}. \tag{6}$$

Since this applies for any $\langle i|$, the general Hamiltonian can be expressed as

$$H = \sum_i |i\rangle\epsilon_i\langle i| + |i\rangle u_{i,i-1}\langle i-1| + |i\rangle u_{i,i+1}\langle i+1|, \tag{7}$$

which is known as the tight binding Hamiltonian. The elements ϵ_i are effectively what determines the potential profile of our system, so these parameters are determined through our choice of barrier in the barrier area.

2.2.3 The energy eigenvalues and energy eigenstates

The energies ϵ_i and hopping elements $u_{i,i\pm1}$ are all equal to ϵ_0 and u respectively on the two semi-infinite lattice chains outside the barrier area. Physically, this means that the atoms constructing these chains are equal. In order to find the eigenenergies on these lattice chains we write the Hamiltonian as two matrices, one for the left semi infinite chain and one for the right. The matrix elements $H_{i,j}$ are $\langle i|H|j\rangle$, which by eq (7) gives the tridiagonal matrices

$$H_{\text{left}} = \begin{bmatrix} \ddots & \ddots & & \dots & 0 \\ \ddots & \ddots & \ddots & & \vdots \\ & \ddots & \epsilon_0 & u & \\ \vdots & & u & \epsilon_0 & u \\ 0 & \dots & & u & \epsilon_0 \end{bmatrix}, \quad H_{\text{right}} = \begin{bmatrix} \epsilon_0 & u & & \dots & 0 \\ u & \epsilon_0 & u & & \vdots \\ & u & \epsilon_0 & \ddots & \\ \vdots & & \ddots & \ddots & \ddots \\ 0 & \dots & & \ddots & \ddots \end{bmatrix}. \tag{8}$$

It is well known (Silvia Noschese and Reichel 1982) that the eigenvalues of a corresponding finite tridiagonal matrix with $N \times N$ entries are on the form $E_k = \epsilon_0 + 2u\cos(ka/(N+1))$. Here k is an index from 0 to N counting the eigenvalues. In the case where N goes to infinity, as is the case for our Hamiltonian matrices, we get a continuous spectrum of eigenenergies

$$E(k) = \epsilon_0 + 2u\cos(ka). \tag{9}$$

The k interval $[-\pi/a, \pi/a]$ is the 1st Brillouin zone, and spans an energy band from $\epsilon_0 - |2u|$ to $\epsilon_0 + |2u|$. The energy eigenstates $|\psi_E\rangle$ are Bloch functions on the form

$$|\psi_E\rangle = \sum_j e^{ikja}|j\rangle, \tag{10}$$

where E denotes the corresponding eigenenergy of the state. This is proven by showing that $|\psi_E\rangle$ solves the time independent Schrödinger equation, and yields the same energy band as eq (9). We have

$$\begin{aligned} H|\psi_E\rangle &= \left(\sum_i |i\rangle\epsilon_0\langle i| + |i\rangle u\langle i-1| + |i\rangle u\langle i+1|\right)\sum_j e^{ikja}|j\rangle \\ &= \sum_j e^{ikja}|j\rangle\left(\epsilon_0 + ue^{ika} + ue^{-ika}\right) \\ &= (\epsilon_0 + 2u\cos(ka))\sum_j e^{ikja}|j\rangle \qquad (11) \\ &= E(k)|\psi_E\rangle \qquad (12) \end{aligned}$$

which proves that $|\psi_E\rangle$ are the energy eigenstates. This also relates k to a physical property, the particle momentum, instead of simply being an arbitrary index for the eigenenergy.

In the limit of small ka, the Taylor expansion of $E(k)$ to second order gives the equation $E(k) \approx \epsilon_0 + 2u - ua^2k^2$. By cleverly choosing $\epsilon_0 = -2u$, the energy resembles that of a free particle

$$E(k) \approx -ua^2k^2 = \frac{\hbar^2k^2}{2m^*}. \tag{13}$$

The hopping amplitude is determined as $u = -\hbar^2/2a^2m^*$, where m^* is the effective mass of an electron moving inside the crystal, assumed to be 0.067 times the actual electron mass . This means that in the limit of small ka, the behavior of an electron in this lattice is analogous to that of a free electron.

2.3 Time independent solution with Green's functions

We define the barrier area from $|0\rangle$ to $|N\rangle$. From now on, the orbital basis states $|j\rangle$ are simply treated as positions in our system. In a scattering system, the scattering eigenstates (Støvneng 1991) can be expressed as

$$|\psi_E\rangle = \begin{cases} \sum_j \left(e^{ikja} + r(k)e^{-ikja}\right)|j\rangle & j \leq -1 \\ \sum_j t(k)e^{ikja}|j\rangle & j \geq N+1 \\ \sum_j c_j|j\rangle & 0 \leq j \leq N \end{cases} \tag{14}$$

where the first term describes an incoming and a reflected electron wave on the left side of the barrier, the second term describes a transmitted wave on the right side of the barrier, and the last term gives the values of $|\psi_E\rangle$ inside the barrier. The coefficient $t(k)$ gives the transmission spectrum $T(k)$ by $T(k) = |t(k)|^2$, which is the term we want. We write the scattering state as

$$|\psi_E\rangle = |S_E\rangle + |\phi_E\rangle, \tag{15}$$

where $|S_E\rangle$ is the source term, describing the incoming electron in eq (14), thus taking the form

$$|S_E\rangle = \sum_{j\leq -1} e^{ikja}|j\rangle. \tag{16}$$

The scattered term $|\phi_E\rangle$ needs to contain everything in (14) that is not contained within $|S_E\rangle$. It takes the form

$$|\phi_E\rangle = r(k)\sum_{j\leq -1} e^{-ikja}|j\rangle + t(k)\sum_{j\geq N+1} e^{ikja}|j\rangle + \sum_{j=0}^{N} c_j|j\rangle. \tag{17}$$

Although $|\phi\rangle_E$ is defined inside the barrier, we are not interested in this term. To obtain the reflection and transmission probabilities we need to solve the Schrödinger equation $H|\psi_E\rangle = E|\psi_E\rangle$ for $|\phi_E\rangle$. We insert eq (15) and write it as

$$(E - H)|\phi_E\rangle = -(E - H)|S_E\rangle. \tag{18}$$

To isolate $|\phi_E\rangle$ we apply a retarded Green's function $G(z)$ to the left of eq (18) where z is an arbitrary complex number. $G(z)$ is an inverse matrix to $(z - H)$ given that the H matrix takes on values for the entire system. To elaborate on this, since $|\phi_E\rangle$ is defined on the entire system, H operating on $|\phi_E\rangle$, means it can be written as a matrix with elements regarding the entire system. Since $|S(k)\rangle$ is only defined on the left semi-infinite chain, when H operates on it, the matrix formed will have zeros at all elements not concerning the rest of the system. This means $G(E)$ will be an inverse to the $(E - H)$ operator on the left term in eq (18), but not to the one on the right. Thus we get the equation:

$$|\phi_E\rangle = -G(z - H)|S_E\rangle \tag{19}$$

to which we are now tasked to find the matrix elements of G.

2.3.1 Finding the Green's matrix elements

We start by defining a perturbed term as $H' = |l\rangle u\langle l+1| + |l+1\rangle u\langle l|$ and write our Hamiltonian as $H = H^0 + H'$. Since the hopping terms between l and $l+1$ are contained within H', H^0 describes two separate chains split between l and $l+1$. We say H^0 has a cut at $[l, l+1]$. We define G^0 as an inverse to $(z - H^0)$. We have $G(z - H)G^0 = G(z - H^0 - H')G^0$ which by our definitions of G and G^0 becomes $G^0 = G - GH'G^0$, rewritten to give the Dyson equation

$$G = G^0 + G^0 H' G. \tag{20}$$

Alternatively by using $G^0(z - H)G = G^0(z - H^0 - H')G$:

$$G = G^0 + GH'G^0. \tag{21}$$

Since H^0 contains no information across the cut, neither does G^0. This means that all off-diagonal elements in G^0 crossing the cut are zero, (all elements $G^0_{m,n}$ with$m \leq l, n \geq l+1$ and $m \geq l+1, n \leq l$ of G^0 are zero).
We define the diagonal elements of G^0 at a cut as:

$$\begin{aligned} \Gamma^-_l &= G^0_{l,l} \\ \Gamma^+_{l+1} &= G^0_{l+1,l+1} \end{aligned} \tag{22}$$

where the - and + denote that the chain corresponding to G^0 continues to the left and to the right, respectively.

By making a cut at $[l+m-1, l+m]$, we get $H' = |l+m-1\rangle u\langle l+m| + |l+m\rangle u\langle l+m-1|$. With this H', we apply $\langle l+m|$ to the left and $|l\rangle$ to the right of eq (20) to obtain the following expression:

$$\begin{aligned} \langle l+m|G|l\rangle &= \langle l+m|G^0|l\rangle + \langle l+m|G^0\left(|l\rangle u\langle l+m| + |l+m\rangle u\langle l|\right)G|l\rangle \\ G_{l+m,l} &= G^0_{l+m,l} + G^0_{l+m,l} u G_{l+m,l+m} + \Gamma^+_{l+m} u G_{l+m-1,l} \end{aligned}$$

Here $G^0_{l+m,l}$ is zero since it is an off-diagonal element crossing the cut. We are left with

$$G_{l+m,l} = \Gamma^+_{l+m} u G_{l+m-1}. \tag{23}$$

We repeat this process, to find $G_{l+m-1,l}$, making another cut at $[l+m-2, l+m-1]$, and so on, until we eventually reach the diagonal element l, l. This finally leads to

$$G_{l+m,l} = \left(\prod_{j=l+m}^{l+1} \Gamma^+_j u \right) G_{l,l}, \tag{24}$$

which is an expression for any off-diagonal element on the upper half of G, expressed by its diagonal elements and the diagonal elements of G^0 at the cuts. Since G is symmetric due to H being symmetric, the lower half of G has the same values, effectively making eq (24) a way to find any off-diagonal element of G.
To find the diagonal elements $G_{l,l}$ we again use eq (20) with a cut at $[l, l+1]$. We get

$$G_{l,l} = \Gamma_l^- + \Gamma_l^- u G_{l+1,l}. \tag{25}$$

By using eq (24) and setting $m = 1$ we get $G_{l+1,l} = \Gamma_{l+1}^+ u G_{l,l}$. Substituting this into eq (25), and rearranging the terms we obtain:

$$G_{l,l} = \left(\left(\Gamma_l^-\right)^{-1} - u\Gamma_{l+1}^+ u \right)^{-1}, \tag{26}$$

which gives any diagonal element in G expressed by the diagonal elements of G^0 at the cuts.
To find Γ^+ and Γ^-, we take a $G^0_{l,l}$ that correlates to a cut at $[l, l+1]$, and make $G^{00}_{l,l}$ which in addition correlates to a cut at $[l, l-1]$. We then do the same process as we did to arrive at eq (26), but with G^0 instead of G. We get

$$\Gamma_l^- = \left(\left(G_{l,l}^{00}\right)^{-1} - u\Gamma_{l-1}^- u \right)^{-1}. \tag{27}$$

The corresponding H^{00} of $G^{00}_{l,l}$ is a Hamiltonian for two separate chains and a separate atom at l. This means that $\langle l|H^{00}|l\rangle = \epsilon_l$, and $(G^{00}_{l,l})^{-1} = \langle l|z - H^{00}|l\rangle = z - \epsilon_l$. This gives the expression

$$\Gamma_l^- = \left(z - \epsilon_l - u\Gamma_{l-1}^- u\right)^{-1}. \tag{28}$$

Analogously, by doing the process with Γ_l^+ and using eq (21) instead, one obtains

$$\Gamma_l^+ = \left(z - \epsilon_l - u\Gamma_{l+1}^+ u\right)^{-1}. \tag{29}$$

To the left of the barrier area all Γ_l^- are equal, and to the right all Γ_l^+ are equal. Outside the barrier, eq (28) and eq (29) become a quadratic equation with the solution

$$\Gamma = \frac{1}{2u^2}(z - \epsilon_0 \pm \sqrt{(z-\epsilon_0)^2 - 4u^2}). \tag{30}$$

The sign in eq (30) must be chosen so that Γ is continuous in z, and yields a non-negative density of states (Economou 2005). For $z = E(k)$ the sign is positive when considering an electron coming from the left, and negative for an electron coming from the right. For these z values, eq (30) can be rewritten to

$$\Gamma = \frac{1}{u} e^{ika}. \tag{31}$$

Now, we have a process to calculate any matrix element of G. By using eq (30) in eq (28) and eq (29), we can find all Γ^+ and Γ^-. Then we find any diagonal elements of G with eq (26), and use eq (24) to find any off-diagonal elements. Note that in this derivation it was not necessary to specify that z is an eigenenergy of H, for G to be an inverse to $(z - H)$. It will be an inverse as long as the z used in (28) and (29) is the same used in $(z - H)$. This is a subtle, yet important point for solving the time-dependent case.

2.3.2 Finding the transmission spectrum

Next, we find the transmitted state $\phi_E(N+1) = \langle N+1|\phi_E\rangle$. By inserting eq (16) and eq (7) into eq (19):

$$\phi_E(N+1) = -\langle N+1|G\left(z - \left(\sum_i |i\rangle\epsilon_i\langle i| + |i\rangle u\langle i-1| + |i\rangle u\langle i+1|\right)\right)\sum_{j\leq -1} e^{ikja}|j\rangle \tag{32}$$

For $z = E(k) = \epsilon_0 + \cos(ka)$ the expression simplifies to

$$\phi_E(N+1) = ue^{-ika}G_{N+1,0} - uG_{N+1,-1}. \tag{33}$$

By eq (21) with a cut at $[-1, 0]$, $G_{N+1,-1} = G_{N+1,0}u\Gamma^-_{-1}$, and by eq (31) $\Gamma^-_{-1} = e^{ika}/u$. Inserting all this into eq (**??**) we get

$$\phi_E(N+1) = -2iuG_{N+1,0}\sin(ka) \tag{34}$$

By eq (17), for N+1, we have $\phi_E(N+1) = t(k)e^{ik(N+1)a}$ which together with eq (34) gives the following expression for the transmission coefficient:

$$t(k) = -2iuG_{N+1,0}\sin(ka)e^{-ik(N+1)a}. \tag{35}$$

It is possible to solve for the reflection coefficient $r(k)$ by repeating the process for $\phi_E(-1)$, however we can easily obtain the reflection probability once we have t(k), by the correlation: $R = 1 - T$.

2.4 Time dependent solution with Green's functions

To study the time it takes a wave packet to travel through the barrier, we need to solve the time dependent Schrödinger equation. We write it as

$$\left(i\hbar\frac{\partial}{\partial t} - H\right)|\Psi(t)\rangle = 0. \tag{36}$$

To solve (36) we use the Laplace transfrom

$$\int_0^\infty dt e^{-st}\left(i\hbar\frac{\partial}{\partial t} - H\right)|\Psi(t)\rangle = 0. \tag{37}$$

By doing a partial integration with the time derivated term, having $|\Psi(\infty)\rangle = 0$ and also moving terms not dependent on t out of the integral, we get

$$-e^{-st}i\hbar|\Psi(0)\rangle - (s\cdot i\hbar + H)\int_0^\infty e^{-st}dt|\Psi(t)\rangle = 0 \tag{38}$$

By rewriting the arbitrary complex number s as $-iz/\hbar$ where z is still an arbitrary complex number, and introducing $\tau = t/\hbar$ as a new measure of time, we obtain

$$-e^{iz\tau}i\hbar|\Psi(0)\rangle + (z - H)\int_0^\infty e^{iz\tau}d\tau\hbar|\Psi(\tau)\rangle = 0. \tag{39}$$

We apply the same retarded Green's function $G(z)$ as derived from 2.2.1. Since $|\Psi(\tau)\rangle$ is defined on the entire system, it will be an inverse to the $(z - H)$ operator. We rearrange some terms to get

$$\int_0^\infty e^{-iz\tau}d\tau|\Psi(\tau)\rangle = e^{-iz\tau}iG(z)|\Psi(0)\rangle \tag{40}$$

to which we can now solve for $|\Psi(t)\rangle$ by taking the Laplace inverse. The Laplace inverse is taken by doing a complex integral around the poles of the function. The matrix $G(z)$ has singularities when z is equal to the eigenvalues $E(k)$. This means $iG(z)|\Psi(0)\rangle$ has poles on the real line within the interval of $E(k)$. We name the path taken around this interval for P, so the final expression takes the form.

$$|\Psi(\tau)\rangle = \oint_P dz\frac{1}{2\pi}e^{-iz\tau}iG(z)|\Psi(0)\rangle. \tag{41}$$

Now by eq (41) we have a way to calculate the state for any time τ given an initial state $\Psi(0)\rangle$. All information of the potential profile in the system lies within $G(z)$. Thus by making an initial wave packet $|\Psi(0)\rangle$, we can use eq (41) to simulate any tunneling event.

2.4.1 Constructing an initial wave packet $|\Psi(0)\rangle$ with minimal uncertainty

We make the initial wave packet $|\Psi(0)\rangle$ by writing it as a linear combination of plane wave states travelling to the right, located on the left semi-infinite chain.

$$|\Psi(0)\rangle = \sum_{j\leq -1} c_j e^{ikja}|j\rangle \tag{42}$$

The coefficients c_j are determined through the desired traits for the wave packet. We wish the wave packet to have a minimal uncertainty product with respect to the Heisenberg uncertainty principle, meaning

$$\Delta x \Delta k = 1/2. \tag{43}$$

This is only the case if the coefficients c_j are chosen (Støvneng 1991) so that eq (42) has the form of a Gaussian distribution,

$$P(x) = \frac{1}{\Delta x\sqrt{2\pi}} e^{-\frac{1}{4}\left(\frac{x-\langle x\rangle}{\Delta x}\right)^2}. \tag{44}$$

Here Δx is the standard deviation and $\langle x\rangle$ is the average position. Given that the wave packet in eq(42) occupies S sites from $j = 0$ to $j = -S + 1$, c_j must fulfill

$$|c_j|^2 = \frac{(S-1)!}{(S-1+j)!(-j)!2^{S-1}}, \tag{45}$$

which in the limit $S \to \infty$ becomes

$$\lim_{S\to\infty} |c_j|^2 = \sqrt{\frac{2}{\pi(S-1)}} \cdot e^{-\left(\frac{2(j+(S-1)/2)^2}{S-1}\right)}. \tag{46}$$

By comparing eq (46) with eq (44) we find that the average position is expressed as $\langle x\rangle = -(S-1)/2$, and the standard deviation is

$$\Delta x = \sqrt{\frac{S-1}{4}}. \tag{47}$$

Thus by inserting eq (45) into eq (42) we get

$$|\Psi(0)\rangle = \sum_{j\leq -1}^{-S+1} \left(\frac{2}{\pi(S-1)}\right)^{\frac{1}{4}} \cdot e^{-\left(\frac{(j+(S-1)/2)^2}{S-1}\right)} e^{ikja}|j\rangle \tag{48}$$

For a more detailed understanding of this inital wave packet see, (Støvneng 1991)

The relation between the standard deviation for the momentum wavenumber k and number of sites S is calculated by using eq (43) and eq (47). We have

$$S - 1 = \frac{1}{\Delta k^2} \tag{49}$$

A fourier transform of $|\Psi(0)\rangle$ gives a wave packet $|\Phi(k)\rangle$ for k space. The wave packet $|\Phi(k)\rangle$ is also a Gaussian, due to the fourier transform of Gaussian's being Gaussian's. This enables us to ensure that 99.7% of the wave packet is within an interval of $[k_0 \pm k_{int}]$ in k space by letting $3\Delta k = k_{int}$ in eq (49), and solve for S. This is calculated to ensure a predictable behaviour of the wave packet when it interacts with the potential barrier.

3 Method

To acquire the necessary data, two python programs was created. One is for solving eq 35 to obtain transmission spectra and the other is for solving eq 40 to simulate time evolution of a system for

an initial wave packet created in accordance with eq 48. The calculations of transmission spectra usually took less than a second while a simulation of time evolution took up to sixteen hours. Thus in order to save time, the cases where simulation of time evolution was required, a search for ARSLs with desired transmission spectra was conducted beforehand.

The system is numerically discretized so that a numerical point corresponds to a lattice point in the tight binding model. We make the ARSLs on the interval $[0, N]$. The entire interval is filled with alternating barriers and wells. The Gaussian distribution expressed as

$$V_0 \exp\left(-\frac{(j - N/2)^2}{\sigma^2}\right)$$

is used to determine the potential height/depth of a barrier or well starting at position j. We define $\sigma = N/4$, where N is the total number of lattice points in an ARSL. The barriers and wells peaks near $N/2$ to a potential of $+V_0$ and $-V_0$ respectively. We define c as the number of lattice points in the barriers and b as the number of lattice points in the wells.

To obtain ARSLs with desired transmission spectra the parameters c, b, V_0 and N were adjusted. Due to calculations of these spectra taking less than a second, it was practical to test lots of various combinations to obtain the desired characteristics. It is not within the scope of this project to make a systematic overview of how the parameters V_0, c, b and N affects transmission spectra. However it is worth to mention that varying N did not change any main characteristics of transmission spectra, but only affects how sharply the transmission transitions from 0% to 100%, and vice versa, which was a useful insight into making desired ARSLs.

To study the time delay due to resonant tunneling, wave packets was sent with 100% transmission probability through ARSLs. By only varying N and keeping all other parameters constant, 100% transmittance was always guaranteed due to the transmission characteristics being unfazed under variations of N. This allowed us to study how the number of barriers inside of ARSLs affects the time delay. To find a comparable way of measuring the traveling time, the integral of the absolute square of the wave packet was calculated over a fixed interval and plotted over time τ. We assume that when this integral yields a value of less than 0.01, it is due to at least 99% of the wave packet having traveled past this interval. Thus by recording the time this happens, we obtain a comparable traveling time.

4 Results and Discussion

4.1 ARSL in series with a single potential barrier

To study a system of a barrier in series with an ARSL, the potential in figure 2, was used to create the (green) transmission spectrum in figure 3. Another potential corresponding to figure 2, where the barrier was instead placed 100 lattice points to the right, was used to create the (green) transmission spectrum of figure 4. The individual transmission spectra of the ARSL (blue) and barrier (orange) was plotted together with the combined system to obtain a systematic overview.

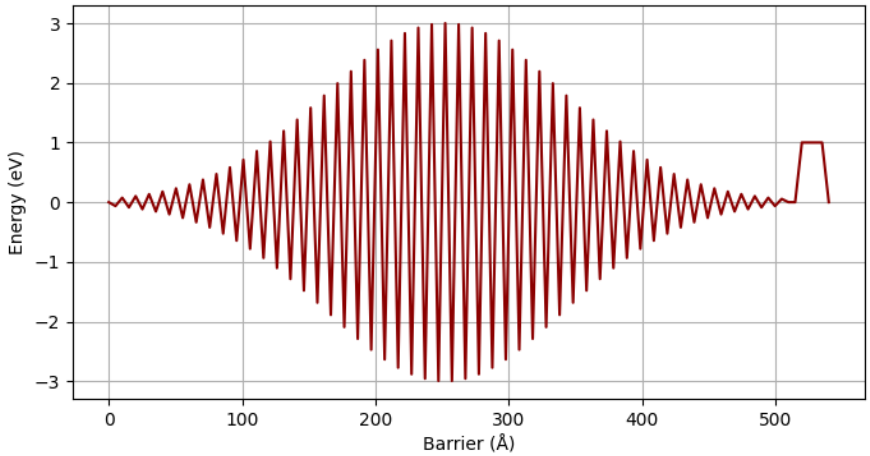

Figure 2: An ARSL with V_0=3eV, c=1, b=1 and N=100 and a barrier placed right behind with V_1=1eV and a thickness of 4 lattice points. Note that the barriers are not actually slanted, this is merely an unfortunate side effect of the way they are plotted.

In both figure 3 and figure 4, it is clear that the transmission spectrum for the combined system overlaps with the transmission spectrum of the barrier, so long the transmission of the ARSL is 100%. In the area where the transmission of the ARSL is 0%, the transmission of the combined system is 0% as well. Due to this being so clear in both figures, it suggests that this characteristic is unaffected by the distance between the ARSL and the barrier. In the relatively short interval where the ARSL transitions between 100% and 0% transmission it displays a non-trivial behavior of rapid oscillations.

It was unexpected that the behavior of the combined transmission spectra would be this simple, since addition of a barrier to other potentials such as another barrier usually yields non-trivial behavior for the entire spectrum. However in figure, 3 and 4, it is clear that any non-trivial behavior is restricted to the area where the ARSL transitions from 100% to 0% transmission. To further test this, a new transmission spectrum figure5 was constructed with an ARSL with a sharper transition, which was accomplished by increasing N to 500. We would expect the interval of non-trivial behavior to be shorter.

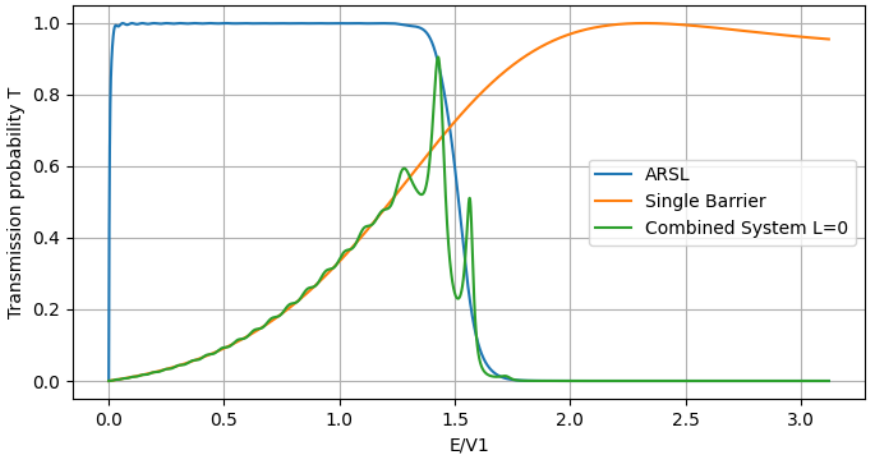

Figure 3: (Green) shows the transmission spectrum of the potential in figure 2. (Blue) and (Orange) shows respectively the transmission for the ARSL and barrier seperately.

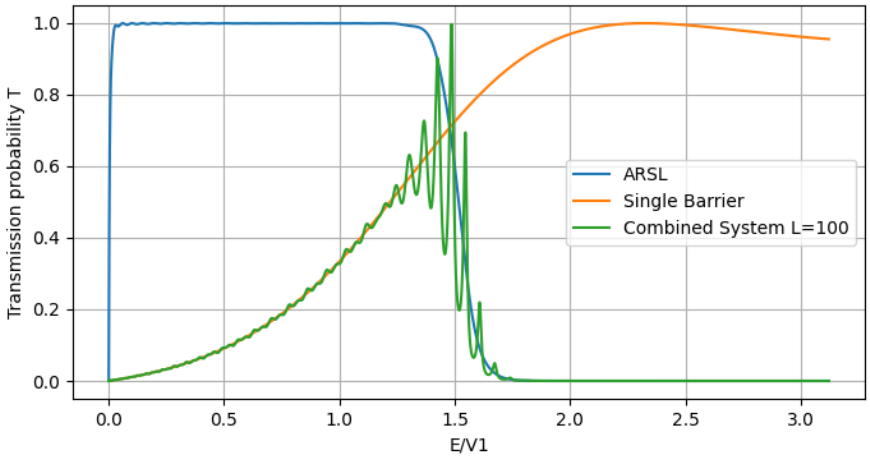

Figure 4: (Green) shows the transmission spectrum of the potential in figure 2 except the barrier has been moved 100 lattice points to the right. (Blue) and (Orange) shows the transmission spectra for the ARSL and barrier separately.

It is clear in figure 5 that by having an ARSL with a sharper transition, the non-trivial behavior is confined to an even shorter interval. This is an interesting result as it indicates that the non-trivial behavior that arises when combining ARSL in series with barriers can be kept to a minimum by arbitrarily increasing N.

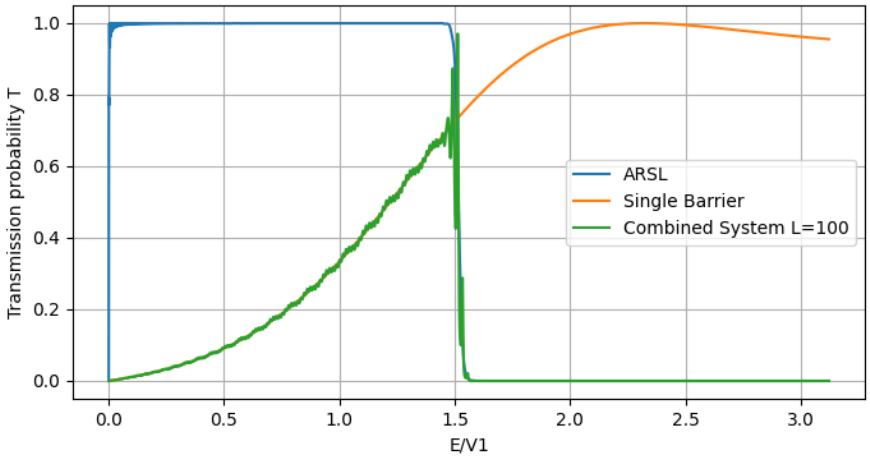

Figure 5: (Green) shows the transmission spectrum of the potential in figure 2 except with $N = 500$ instead of 100, and the barrier has been moved 100 lattice points to the right. (Blue) and (Orange) shows the transmission spectra for the ARSL and barrier separately.

To minimize the possibility that this effect is only restricted to an ARSL and barrier with the specific parameters in figure 2, transmission spectra for other ARSLs and barriers were tested like the one showed in figure 6.

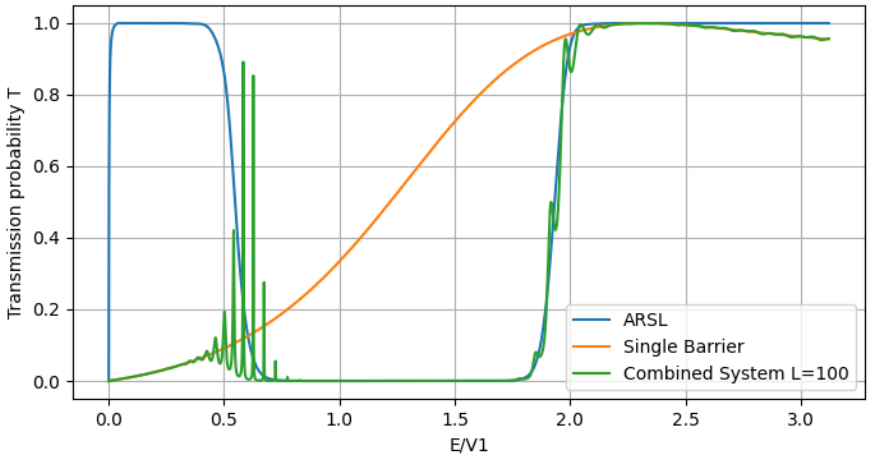

Figure 6: Transmission spectrum from an ARSL with $V_0 = 1$eV, $c = 1$, $b = 1$, $N = 100$ and a barrier with V_1 1.5eV and thickness of 4 lattice points lattice points placed 100 lattice points to the right

Combinations of ARSLs with N ranging from 100 to 1000, c and b ranging from 0 to 4 and V_0 ranging from 1 to 3 eV were tested in series with different barriers with V_1 ranging from 1 to 3 and barrier thickness ranging from 0 to 4, placed anywhere from right behind the ARSL up to 1000 lattice points to the right. They all display the same characteristic behavior mentioned previously.

It was also attempted to mirror these systems, placing the barrier in front of the ARSLs instead. They all yielded the same transmission spectra for when it was placed behind. It is unknown whether this is a characteristic of ARSLs specifically, or a general behavior in quantum tunneling.

For further work, it would be interesting to study how ARSLs ineracts when placed in series with other potentials to see if the characteristic effects displayed here is due to a general property of ARSLs.

4.2 Tunneling delay time for an ARSL

To study the tunneling delay time, ARSLs with the same parameters as that in figure 2 were used, except for N which varies depending on the simulation. Simulations were run to study the tunneling delay time through this ARSL for $N = 50$, $N = 100$, $N = 200$, $N = 500$ and one where there were no potential at all, which could be used as a reference point. The average energy of the electron wave packet was set to 0.36eV, which is less than a fifth of V_0. Figure 7 highlights where in the transmission spectrum we are sending these wave packets. By having $S = 200$ for the initial wave packet, see eq 48 we guarantee that the entire packet is within the 100% transmission area of the ARSLs with the N values used.

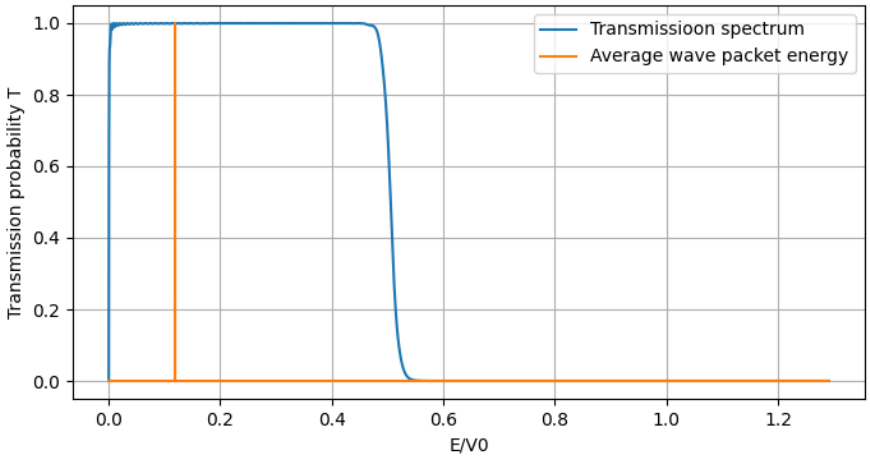

Figure 7: Transmission spectrum of an ARSL that has N=200 V_0=3eV, c=1 and b=1. The vertical (Orange) line highlights the average energy of the incoming electron wave packet.

The interval of the system is always between 0 and 4000 Å (0 and 800 lattice points). The initial wave packet is placed at 500Å and the barriers always start at 1000Å. Figure 8 illustrates an example of the setup for the ARSL with $N = 200$.

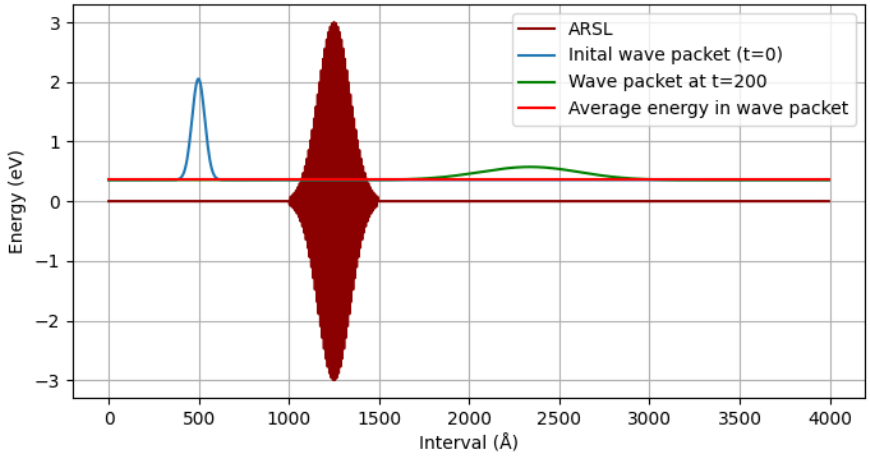

Figure 8: An illustration showing a wave packet at two different time frames, traveling through the ARSL with $N = 200$. The wave packets are plotted so that their base is at the their average energy of 0.36eV

The time τ when 99% of the wave packets has left the interval (0 to 4000Å), was used as the comparable traveling time. The data is presented in table 1 and figure 9.

Table 1: Travel time for a system of 800 lattice points for ARSLs with varying N. Travel time was calculated by finding the time step for which 99% of the wave packet had left the system

Length of ARSL	Travel time τ
N=0 (No barrier)	664
N=50	652
N=100	640
N=200	612
N=500	536

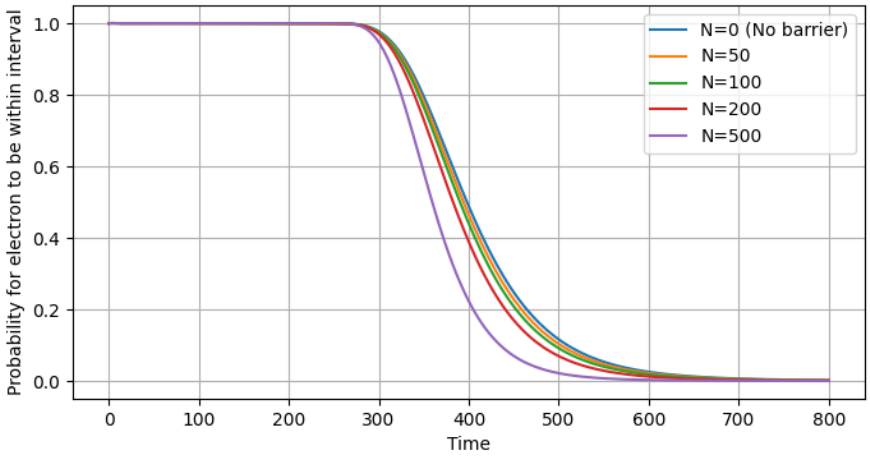

Figure 9: The integral over the interval 0 to 4000Å of the absolute square of wave packets traveling through ARSLs with varying N, plotted for time τ.

Table 1, shows a clear indication that the electron travels faster through ARSLs than no barrier. It also shows a trend of higher N in an ARSL, gives shorter traveling times. This was the opposite of what was expected, as it was assumed that ARSLs would give a tunneling delay time comparable to that of a double barrier. A possible explanation is that ARSLs and double barriers are not comparable in this regard due to the ARSLs having wells between its barriers while a double barrier does not. To test this, a second set of simulations were run with the same setup, but setting the potential in all of the wells of the ARSLs to 0, effectively removing them. Thus we expect the second set of simulations to yield a delay in traveling time which increases with N due to the wells being removed. Ideally, we would not want to make any further changes to the ARSLs, since this adds a layer of uncertainty when comparing the second set of results with that in table 1. However by removing the wells, the transmission spectra no longer yielded 100% transmission for 0.36eV, so V_0 was also adjusted to 0.2eV to account for this giving the transmission spectrum in figure 10.

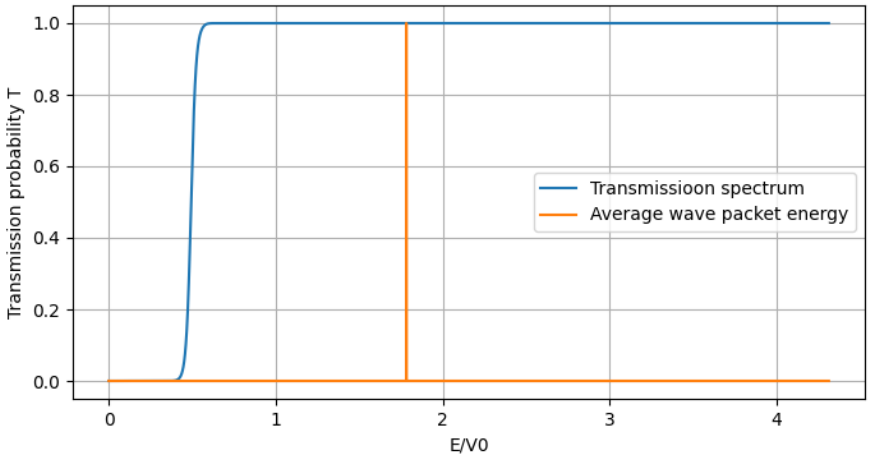

Figure 10: Transmission spectrum for the ARSL with removed wells, and V_0 adjusted to 0.2eV. The vertical (Orange) line highlights the average energy of the incoming electron wave packet.

The data from the second set of simulations is presented in table 2 and in figure 11. It should also be noted that since the particle energy is higher than the potential this is technically no longer quantum tunneling.

Table 2: Travel time for second set of simulations. The wells in the ARSLs has been removed, and V_0 set to 0.2eV. Travel time was calculated by finding the time step for which 99% of the wave packet had left the system

Length of ARSL	Travel time τ
N=0 (No barrier)	664
N=50	654
N=100	672
N=200	708
N=500	837

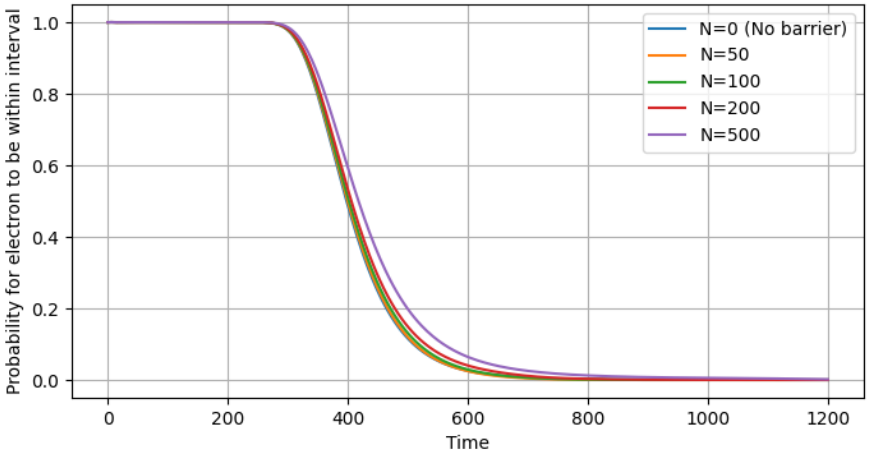

Figure 11: The integral over the interval 0 to 4000Å, of the absolute square of wave packets traveling through ARSLs without wells for the second set of simulations.

From table 2, we can see the traveling time for the second set of simulations increases with N, for $N = 100$ and greater, which was expected. It was however unexpected that the traveling time once again was shortened for $N = 50$. This was likely due to the transmission spectra for the ARSL without wells, having less of a clean 100% transmission area for low N, meaning some of the wave packet was likely reflected. Given that a part of a wave packet is reflected, it will leave the interval earlier since the distance traveled to the left is shorter than to the right. Due to the nature of how the travel time is calculated this error leads to a shorter traveling time. Upon further inspection, this suspicion was confirmed by plotting the system for $N = 50$ at time $\tau = 240$ (figure 12), where a reflected part can be seen at the bottom left. By integrating the absolute square of only the reflected part, it showed that about 0.5% of the wave packet had been reflected. For comparison, the same analysis was made for $N = 100$, where it was calculated that less than 0.05% had been reflected. Thus we choose to rule out $N = 50$ for the second set of simulations, while keeping the rest when forming our conclusion.

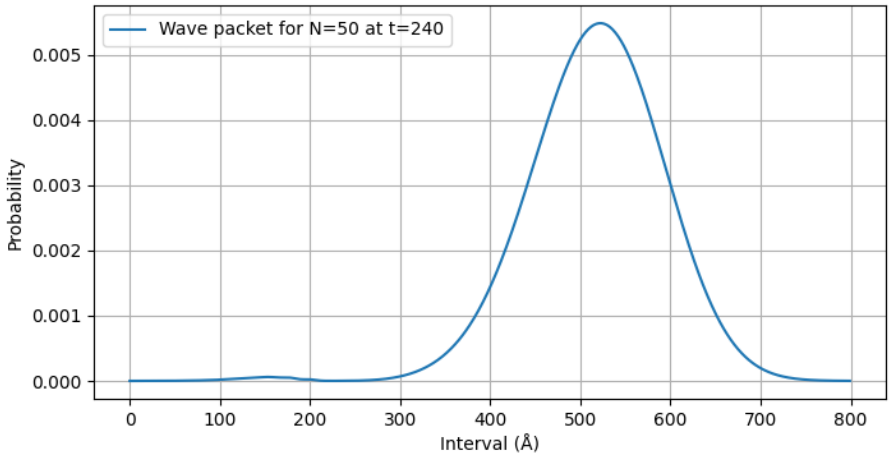

Figure 12: Wave packet from second set of simulations for $N = 50$ plotted at $\tau = 240$. The larger wave to the right has mostly passed the barrier, while a reflected part can be seen at the bottom left.

The second set of simulations with the removal of barriers shows a trend of increased traveling time with increasing N, as we would expect when comparing to a double barrier. However due to V_0 simultaneously being reduced in the second set of simulations, it is not possible to conclude certainly that this is due to the removal of wells, the decrease in V_0, or a combination of the two. Nonetheless we can only conclude that this somewhat gives an indication that it is the inclusion of wells between the barriers in ARSLs that drives the tunneling time down. This should be studied further to make a certain conclusion.

The first set of simulations clearly displayed that the traveling time goes down with increasing N in ARSLs. However it is unclear whether this correlation means that the electron's traveling speed inside an ARSL increases with the parameter N, or if it simply travels at a fixed yet higher speed inside an ARSL. The latter gives the same correlation due to the wave traveling with this higher fixed speed for longer parts of the interval with increasing N. This distinction would also be interesting to find in a further study.

4.3 Trapping an electron between ARSLs

Two ARSLs with the parameters $V_0 = 0.4$eV, c =3, b =2 and $N = 100$ are used to trap an electron wave packet with an average energy of about 0.9 eV. The transmission spectrum for these ARSLs is plotted in figure 13 with the average electron energy highlighted.

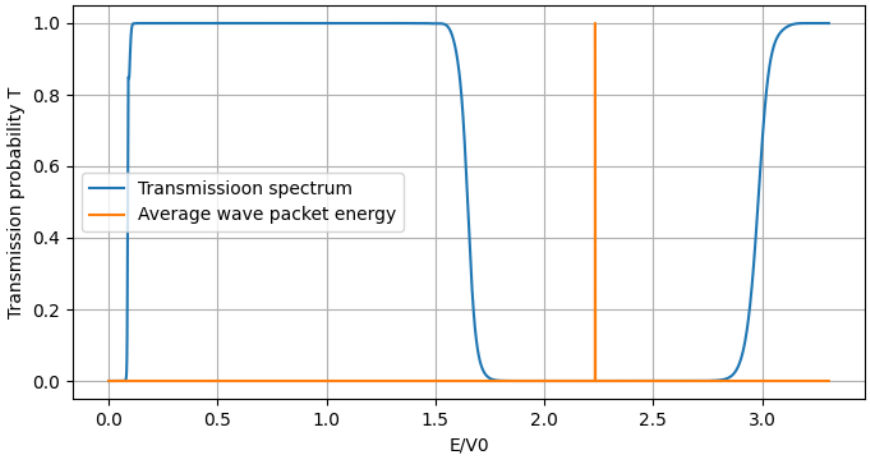

Figure 13: Transmission spectrum of an ARSL with $V_0 = 0.4$eV, $c = 3$, $b = 2$ and $N = 100$. The vertical (Orange) line highlights the average energy of the initial electron wave packet.

An initial wave packet was created on an interval with length 4000Å ($S = 800$ in eq 48) between the two ARSLs, to which the time evolution was simulated up to $\tau = 15000$. This was done for no other reason than to highlight the unintuitive properties of ARSLs in an amusing way. In figure 14, we can see the electron at $\tau = 2000$ and $\tau = 15000$ after having bounced back and forth countless times. We have effectively trapped an electron with more than twice the amount of energy needed to escape classically.

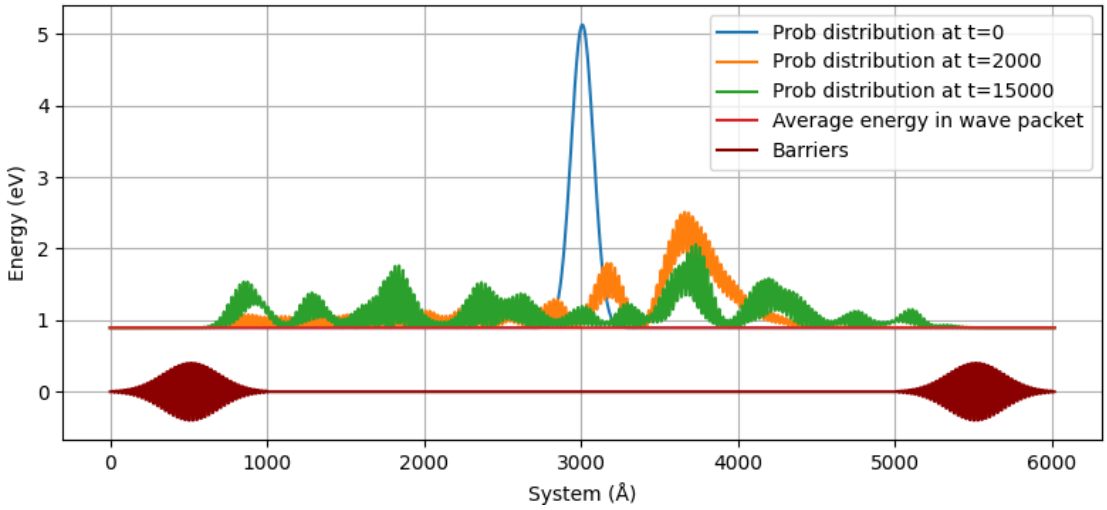

Figure 14: An illustration showing different time frames of an electron wave packet trapped between two ARSLs. The wave packets are plotted so that their base is at the their average energy of 0.9eV

The leakage was measured by integrating the absolute square of the wave packet for the entire interval, and plotting over time (see figure 15). For the entire time period up to $\tau = 15000$, less than 3% leaked out of the system.

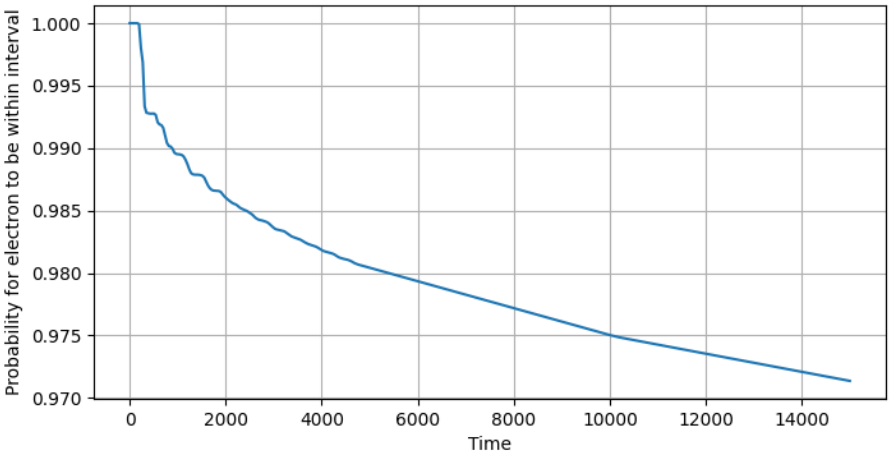

Figure 15: The integral of the absolute square of the trapped wave packet for the entire interval plotted over time τ.

5 Conclusion

With the use of the tight binding model, the transmission and reflection properties of ARSLs were studied and demonstrated through simulations and analyses of their transmission spectra. It was discovered that the parameter N in an ARSL does not influence the main characteristics of its transmission spectrum, but only how sharply the transmission transitions between 0% and 100%.

A system of a potential barrier placed behind or in front of an ARSL was found to yield the transmission spectrum of the barrier in the region where the ARSL yields 100% transmission and 0% transmission when the ARSL yields 0% transmission. In the regions where the ARSL transitions between 0% and 100% transmission the spectrum of the combined system displays a non-trivial behavior.

It was found that tunneling electron wave packets travels faster through an ARSL than no potential at all. It was indicated that this faster traveling time is due to the wells between the barriers, as it is well known that resonant tunneling through a double barrier has a delay time.

Lastly the unintuitive properties of ARSLs were highlighted by trapping an electron between two ARSLs when the electron had more than twice the energy needed to escape classically.

Bibliography

Economou, E. N. (2005). *Green's Functions in Quantum Physics*. Springer.

Kittel, Charles (2018). *Kittel's introduction to solid state physics*. Wiley.

Nakagawa, T., N.J. Kawai and K. Ohta (1985). 'Time evolution of electron wave-packets in modulated superlattices and at their boundaries'. In: *Superlattices and Microstructures* 1.3, pp. 217–221. ISSN: 0749-6036. DOI: https://doi.org/10.1016/0749-6036(85)90006-0. URL: https://www.sciencedirect.com/science/article/pii/0749603685900060.

Silvia Noschese, Lionello Pasquini and Lothar Reichel (1982). 'Tridiagonal Toeplitz Matrices: Properties and Novel Applications'. In: *Department of Mathematical Sciences, Kent State University* 48, pp. 387–411.

Støvneng, Jon Andreas (1991). 'Dynamics of Tunneling'. PhD thesis. Norges Tekniske Høgskole i Trondheim NTH, pp. 1–57.

Tung, Hsin-Han and Chien-Ping Lee (1996). 'An energy band-pass filter using superlattice structures'. In: *IEEE Journal of Quantum Electronics* 32.3, pp. 507–512. DOI: 10.1109/3.485403.

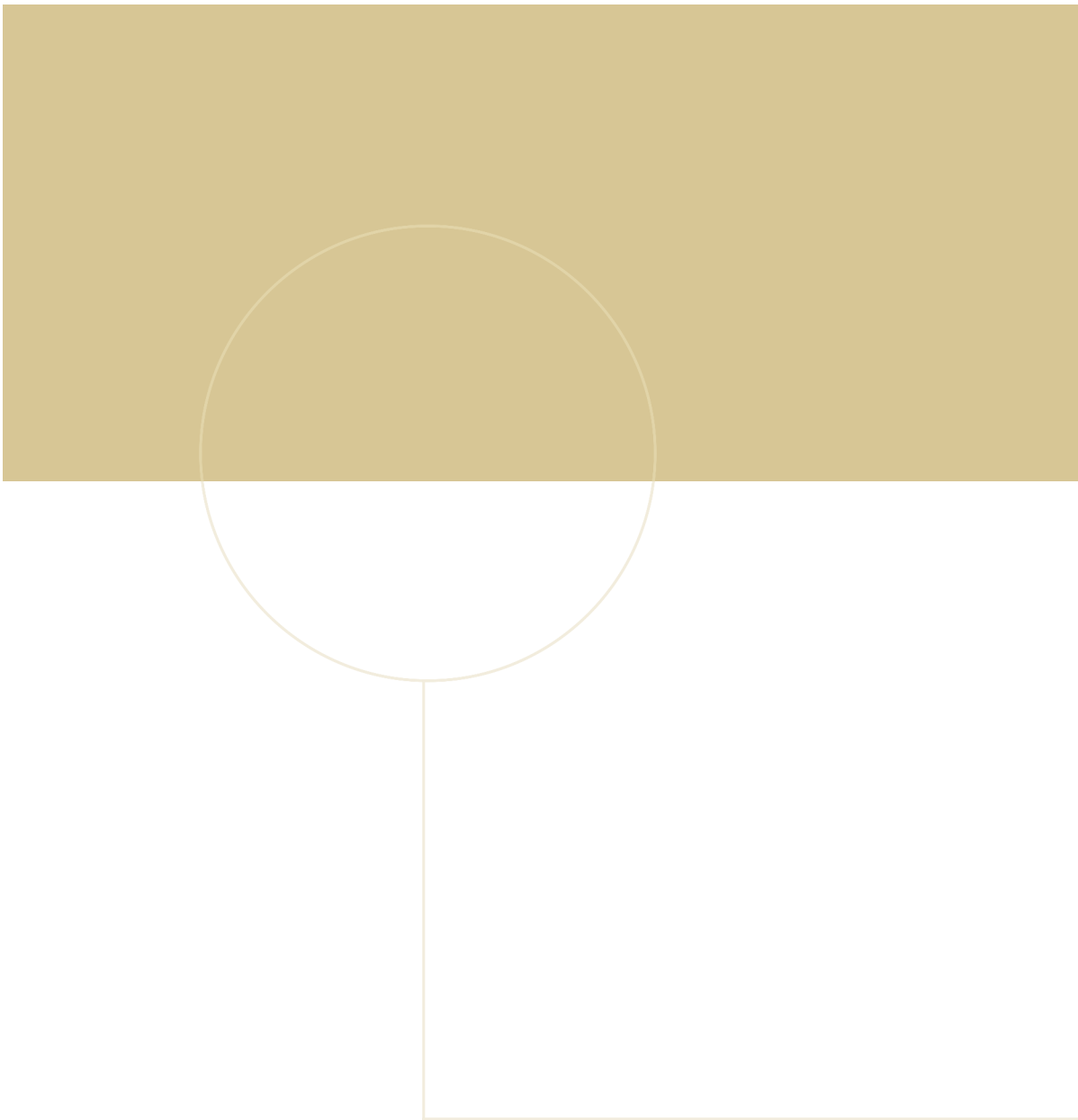

NTNU

Norwegian University of
Science and Technology